Progress In Electromagnetics Research M, Vol. 107, 51–63, 2022

A Compact Dielectric Resonator Based Dual Port Circularly Polarized MIMO Antenna for Wideband Applications

Piyali Chakraborty[1], Utsab Banerjee[3], Anuradha Saha[2], and Anirban Karmakar[1, *]

Abstract—In this communication, a compact Dielectric Resonator (DR) based multiple-input-multiple-output (MIMO) antenna is presented for wideband applications. The antenna consists of two modified kite-shaped monopoles where four DRs have been placed on the patch. Corners of four DRs have been etched to implement the orthogonal phase, which leads to circular polarization characteristics. Implementation of DRs also helps in bandwidth enhancement purpose. Two L-shaped parasitic strips along with a Y-shaped stub have been used in the ground plane so as to obtain high isolation, which leads to a decrease of mutual coupling between the antenna elements. The proposed antenna achieves a wide impedance bandwidth of 7.1–22 GHz (106%) along with low mutual coupling of less than −15 dB within the entire frequency range as well as circular polarization characteristics, which covers the frequency range (−3 dB) of 7.1–7.9 GHz (10.6%). Thus the antenna can be considered as a potential candidate for modern wireless communication systems.

1. INTRODUCTION

Multiple transmitting and receiving antennas with low mutual coupling are used in a multiple-input multiple-output (MIMO) diversity system. This technology increases the data transmission capacity by transmitting and receiving many signals at a time. For this purpose, the interest in MIMO antenna is proficiently increased. On the other hand, in the situation of MIMO antenna misalignment, circularly polarized MIMO systems show better performance and reliability than linearly polarized MIMO systems [1]. For this purpose, a few antenna designs have been reported in the open literature [2–4]. Most importantly, along with circularly polarized MIMO antenna, the implementation of DRs has become the foremost choice as it can enhance bandwidth characteristics. In recent years, it is required to have a high data rate, high channel capacity, and high reliability within the limited power level, which is only possible by using multiple-input multiple-output (MIMO) antenna systems that connect multiple radiators at both transmitter and receiver sides [5, 6]. High isolation in MIMO antenna can be achieved by introducing protruded ground plane, neutralization line, defected ground structure, etc [7–9]. For MIMO applications, printed antennas are more attractive due to their compact size and easy fabrication. But one of the disadvantages of using printed antennas is high metallic loss and high surface wave loss that can be overcome by using Dielectric Resonators (DRs) [10–13].

It has been observed [10] that DRs can be attractive alternatives to low gain antennas such as microstrip patches, monopole, and dipole. It has also been found that DRAs can be considered to be efficient radiators by exciting appropriate mode [14–17].

On the other hand, Circularly Polarized (CP) antennas have advantages such as insensitivity towards equipment orientation, suppression of multipath fading, and resistance towards inclement

Received 14 September 2021, Accepted 20 December 2021, Scheduled 4 January 2022
* Corresponding author: Anirban Karmakar (anirban.ece@gmail.com).
[1] Electronics and Communication Engineering Department, Tripura University, Tripura, India. [2] AEIE Department, Netaji Subhash Engineering College, Kolkata, India. [3] ECE Department, MVJ College of Engineering, Bangalore, India.

weather [18]. Therefore, researchers mainly focussed on wideband circularly polarized antennas for advanced wireless communication systems [19–27].

Lastly, the use of a MIMO antenna is an effective way to increase spectral efficiency and improve link reliability of the radio communication [28–35].

In this article, a new wideband CP DRA-based MIMO antenna for wireless application is presented. The proposed antenna achieves an impedance bandwidth of 7.1–22 GHz, low mutual coupling of less than −15 dB within the entire frequency range, as well as circular polarization characteristics, which covers the frequency range of 7.1–7.9 GHz.

2. ANTENNA DESIGN AND ANALYSIS

The configuration of the proposed antenna is shown in Figs. 1(a)–(e). The overall size of the antenna is $30 \times 33 \times 0.762\,\text{mm}^3$. The monopole is etched on a Roger Duroid 6002 substrate with a dielectric constant (ε_r) of 2.94. The two identical modified kite-shaped monopoles have been placed side by side so as to create better diversity performances. One of the corners of the kite-shaped radiating elements has

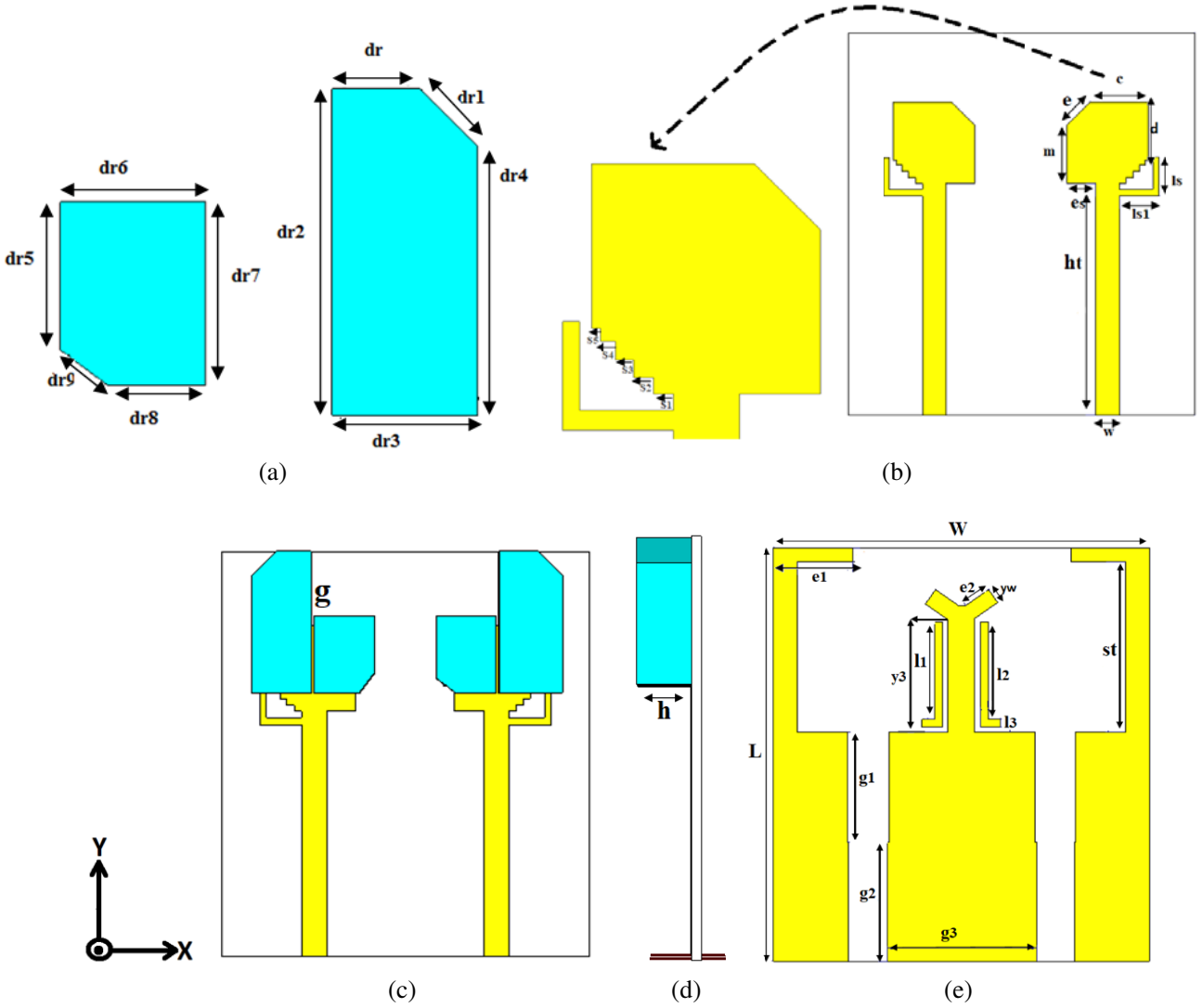

Figure 1. Top view of the proposed antenna: (a) DR, (b) without DR dual port MIMO, (c) proposed antenna, (d) side view of the proposed antenna, (e) back side of the proposed antenna.

Table 1. Dimensions of the proposed antenna.

Symbol	Value (mm)	Symbol	Value (mm)
ht	20	yw	1.2
ls	3.30	$l2$	7.80
$ls1$	3.40	$y3$	8.99
w	2	$e1$	4.40
$l1$	7.80	$e2$	2.2
$l3$	1.60	$g3$	11.92
st	13.60	W	30
$g1$	8.80	L	33
$g2$	9.50	$dr5$	5
dr	3.1	$dr9$	1.5
$dr2$	11.5	$dr7$	6.3
$dr3$	5	h	5.236
$dr1$	1.5	$dr4$	9.6
$s1$	0.5	$s3$	0.5
$s2$	0.5	$s4 = s5$	0.7
$dr8$	4	es	2.5
$dr6$	5.5	m	5
d	5	e	2.5
g	0.2	c	4.5

been cut into stepped shape in order to reduce metallic loss, which also enhances impedance bandwidth as well. A rectangular inverted L-shaped strip has been attached with the monopole to improve the bandwidth performances. Four DRs have been used to lower the Q factor so as to broaden the impedance bandwidth, which covers the frequency range of 7.1–22 GHz. A small gap between the two DRs has been maintained so as to enhance the bandwidth performance. Al_2O_3 has been chosen as DR with dielectric constant of 9.8. DRs have been cut at the corners to intensify circular polarization characteristics as well. Ground plane has been engraved at the backside of the antenna substrate. On the ground plane, an extended Y-shaped stub along with two L-shaped parasitic strips has been used to achieve isolation which reduces the mutual coupling between the two radiating elements. The proposed antenna has been optimized and simulated by using High-Frequency Structure Simulator version 18 (HFSS). The optimized dimensions of the proposed antenna are shown in Table 1. Here, the effective length of the basic monopole (7.9 mm) has been chosen as quarter wavelength at a frequency of 8 GHz, which has been calculated by using Equation (1).

$$d_t = \frac{\lambda_g}{4} = \frac{c}{4 \times f_{res} \times \varepsilon_{eff}} \approx 7.9\,\text{mm} \tag{1}$$

This leads the monopole to the first resonant frequency around 8 GHz which can be seen from Fig. 3(a). Here, c = speed of light, λ_g = guided wavelength, f_{res} = first resonant frequency of the monopole, and $\varepsilon_{eff}(\sqrt{\varepsilon_r + 1/2})$ is the effective permittivity of the substrate.

The resonant frequency of rectangular DRA due to $TE_{11\delta}$ mode is calculated by using dielectric waveguide modal (DWM) method [27] using the following equation:

$$f_o = \frac{c}{2\pi\sqrt{\varepsilon_{dr}}} \times \sqrt{k_x^2 + k_y^2 + k_z^2} \tag{2}$$

where c is the speed of light in vacuum; k_x, k_y, and k_y are the wave numbers of the DR in x, y and z directions, respectively.

3. RESULTS AND ANALYSIS

The S_{11} characteristics from the evolution of the proposed antenna are shown in Fig. 3(a). The S_{21} characteristics of the isolation structure are shown in Fig. 3(b). In Fig. 3(a), it is observed that by implementing a modified kite-shaped MIMO antenna, impedance matching at the lower bandwidth is improved, whereas the upper frequencies of the S_{11} bandwidth remain almost unchanged. To excite an additional resonance at the frequency of 10 GHz, an inverted L-shaped strip has been added with the kite-shaped monopole so as to cover the lower end bandwidth as shown in Fig. 3(a). Fig. 2 presents the surface current distribution at 10 GHz when port 2 is excited. It is observed that a large amount of surface current is concentrated in the inverted L-shaped strip which acts as a resonator that in turn helps in enhancing the lower end bandwidth. Moreover, the overall impedance bandwidth has been improved by implementing different structural elements of the MIMO antenna along with DRs.

In Fig. 3(b), it is seen that S_{21} bandwidth (isolation characteristics) is enhanced after implementing a Y-shaped stub along with L-shaped parasitic strips. Hence, from the figure, it can be concluded that the proposed isolation structure providing isolation from 7.1 to 22 GHz (< -15 dB).

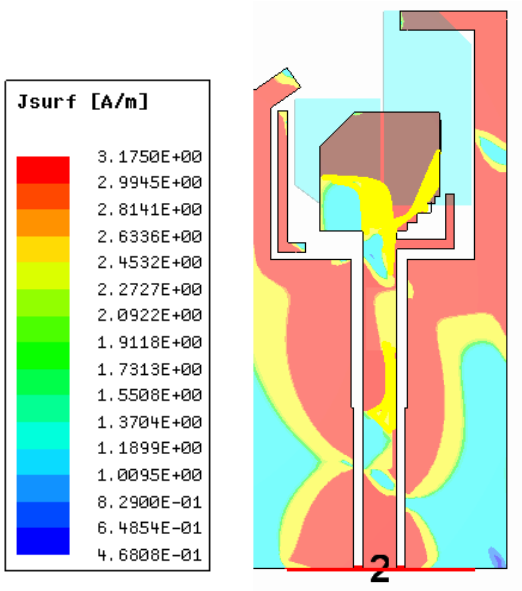

Figure 2. Current distribution on the L-shaped strip at 10 GHz at port 2.

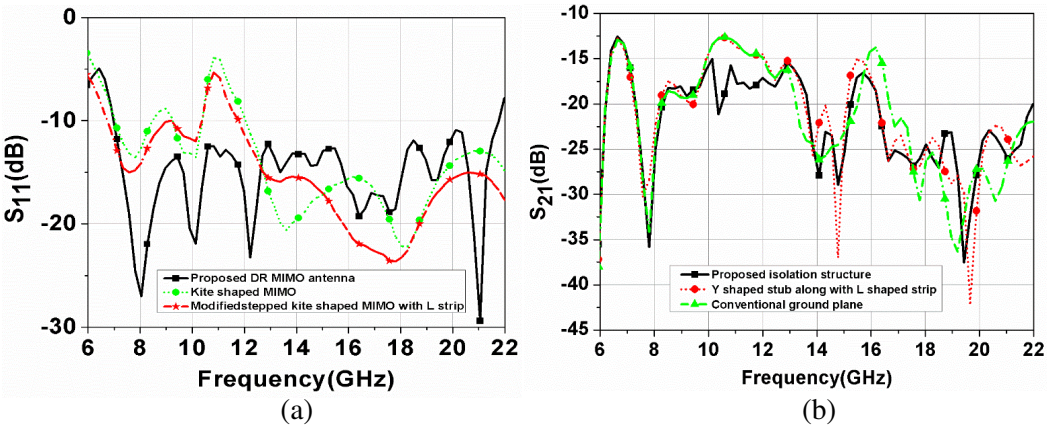

Figure 3. Comparison of S_{11} and S_{21} characteristics. (a) S_{11} characteristics for different stages of the antenna. (b) S_{21} characteristics for different stages of the isolation structure.

The Axial Ratio (AR) [11] which accounts for the quality of CP has been obtained by the following equation:

$$\mathrm{AR\,(dB)} = 20\log\frac{E_{\max}}{E_{\min}} \tag{3}$$

Here, AR is the ratio of the major to minor axes of polarization along the bore-sight of the proposed antenna, which is derived from the measured results. $E_{\max}$ and $E_{\min}$ are spatially orthogonal field components. The AR bandwidth of the antenna is chosen to be the frequency range (=< 3 dB), which satisfies the −3 dB cut-off. It is observed from Fig. 4 that the axial ratio bandwidth gets narrower without implementing DRs. After the implementation of DR, axial ratio bandwidth of 7.1–7.9 GHz has been achieved. So, at the frequency range of 7.1–7.9 GHz, the antenna is circularly polarized, whereas the antenna is linearly polarized for the remaining frequency range of 7.1–22 GHz, and the usability of the antenna can be fixed accordingly as per the polarization along with operating frequency.

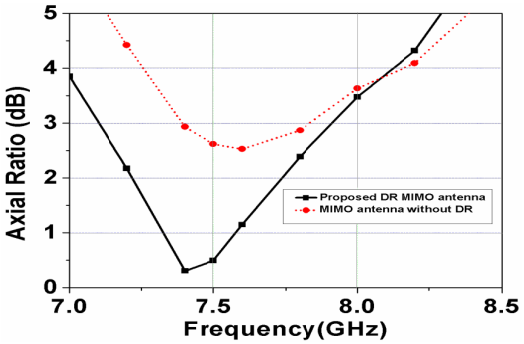

Figure 4. Axial ratio bandwidth of the proposed antenna.

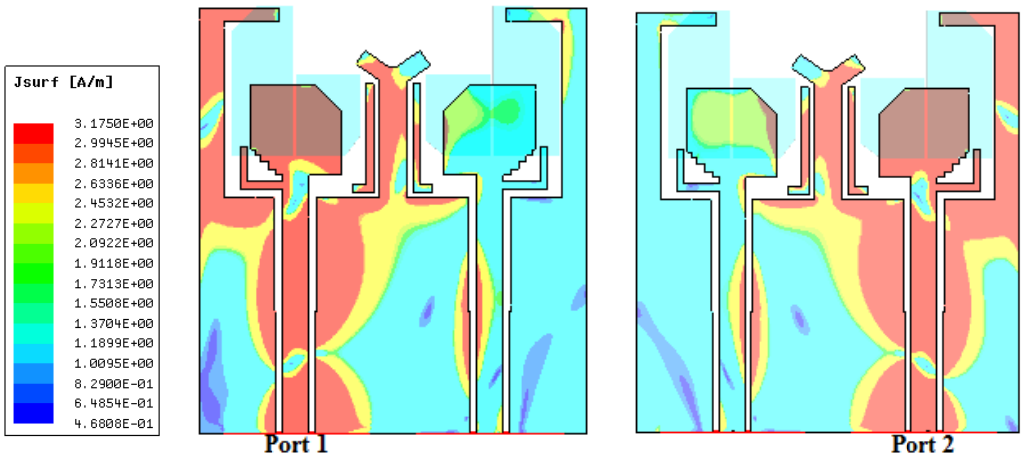

Figure 5. Surface current distribution of the proposed antenna at 7.5 GHz: (a) port 1 is excited, (b) port 2 is excited.

Figures 5(a)–(b) present the surface current distribution of the proposed antenna. The effectiveness of decoupling between the radiating elements is demonstrated. The current distributions are obtained when port 1 and port 2 are excited at 7.5 GHz. It is seen that the coupling current flowing from port 1 to port 2 gets suppressed, which leads to reduced mutual coupling. It is also observed that the current in the centre of the ground plane is very weak. The inclusion of a Y-shaped stub along with two L-shaped parasitic strips in the ground plane improves the antenna's isolation by expanding the electrical length.

As a result, most of the surface current is concentrated in the isolation structure which in turn provides about −15 dB isolation across the whole operating band.

Figure 6 presents the electric field distribution at 7.6 GHz inside DRs at different time phases where it is excited by port 2 only. Here, DRs have been cut at the corners to intensify circular polarization characteristics. The dominant electric field vectors inside DRs have been denoted by E_1, E_2, and E_3. The resultant of all the dominant electric field vectors at 0°, 90°, 180°, and 270° is denoted by E_{r1}, E_{r2}, E_{r3}, and E_{r4}, respectively. At 0° phase, it is observed that the representation of resultant vector of all the dominating electric field vector (E_{r1}) points from lower right to upper left corner. As the phase advances from 0° to 90° it is observed that the resultant vector (E_{r2}) points from lower left to upper right corner. Further advancement of phase towards 180° (E_{r3}) and 270° (E_{r4}) displays a clockwise rotation of resultant electric field vector, which leads to LHCP radiation in the $+Z$ direction and RHCP radiation in the $-Z$ direction. Cutting corners of DRs generates some field components (like E_3 in Fig. 6(a)) which in turn intensify the orientation of resultant vectors to be directed properly to create circular polarization.

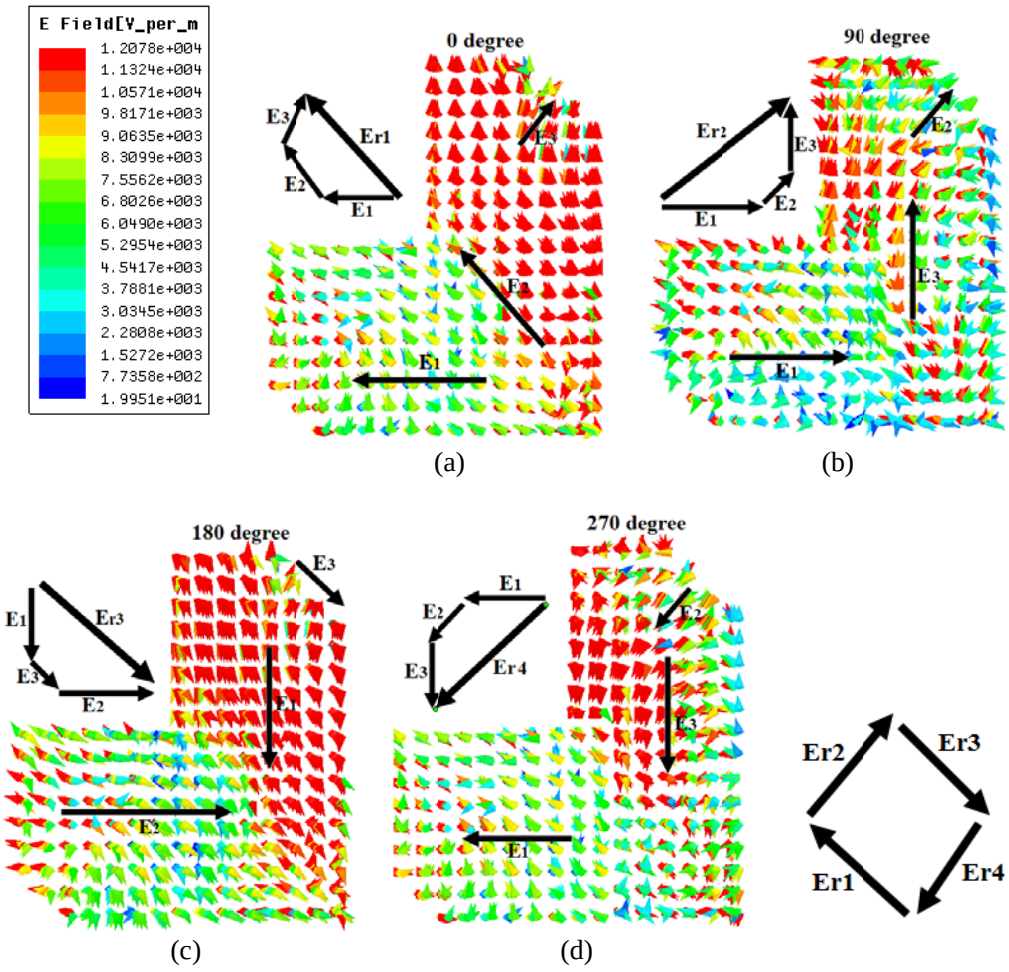

Figure 6. Electric field distribution inside DR at 7.6 GHz at: (a) 0° phase, (b) 90° phase, (c) 180° phase, (d) 270° phase.

4. PARAMETRIC STUDIES

The length of L-shaped strip, which is attached with the patch, is represented as ls. By keeping the length $ls = 2.5$ mm, it is seen that the S_{11} bandwidth becomes narrower. As the length of L-shaped strip (ls) changes from 2.5 mm to 3.3 mm, it is seen that the S_{11} bandwidth is improved highly, which satisfies

the matching performance (< -10 dB). Similarly, it is also observed that the S_{11} bandwidth marginally decreases when the length of ls further changes from 3.5 mm to 4 mm. Therefore, the parameter (ls) is optimally chosen to be 3.3 mm. Hence, it is clear from the analysis that the change of the length of ls affects the S_{11} bandwidth, as shown in Fig. 7. Most importantly, it is also noticed that the impedance matching is also dependent on the stepped monopole along with L-shaped strip. Thus, the modified kite-shaped stepped monopole along with L-shaped strips equally plays an important role to enhance impedance of the monopole.

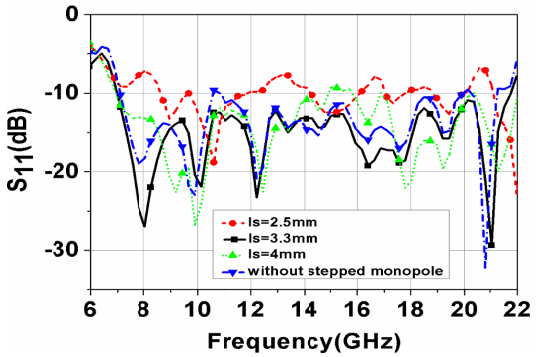

Figure 7. Effect of ls on S_{11} characteristics.

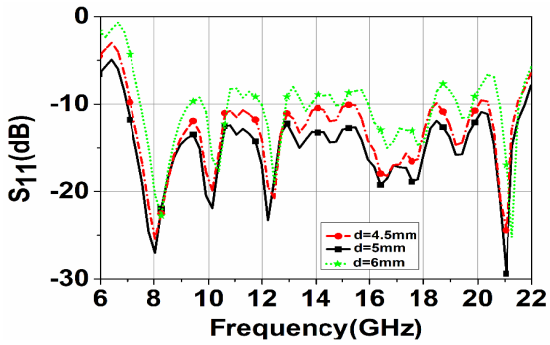

Figure 8. Effect of d on S_{11} characteristics.

As the partial length of the patch (d) changes from 4.5 mm to 5 mm, it is seen that the S_{11} bandwidth gets highly improved, which satisfies the matching performance (< -10 dB). As the length of d increases from 5 mm to 6 mm, it is observed that the bandwidth gets shifted towards the lower end frequency, which affects the overall bandwidth characteristics. Hence, it is clear from the analysis that the change of the length of the patch (d) affects the S_{11} characteristics as shown in Fig. 8. Overall, it is seen that the effect of these parameters on the S_{11} bandwidth is less pronounced than the other parameters shown in the study.

Figure 9 depicts the effect of AR bandwidth by varying the gap (g) between two DRs. Increasing or decreasing the gap between the two DRs degrades the 3-dB AR bandwidth. So, the gap (g) between two DRs is optimally chosen to be 0.2 mm. Keeping the parameter $g = 0.2$ mm lowers the Q factor and broadens the AR bandwidth. The gap is used to reduce the mutual coupling between DRs, which can enhance 3-dB AR bandwidth. Hence, the change of the value of g affects CP performances.

Figure 10 presents the effect on AR bandwidth performance by varying the height (h) of DRs. The effect of variation of the height (h) of DR on antenna performance is studied here to find out the optimal value. As the value of 'h' increases from 4 mm to 5.236 mm, it is seen that the AR bandwidth gets drastically enhanced. It is also noticed that the AR bandwidth is slightly improved as the value of 'h' increases from 4 mm to 5.536 mm. Thus, $h = 5.236$ mm is chosen as an optimal value where the AR

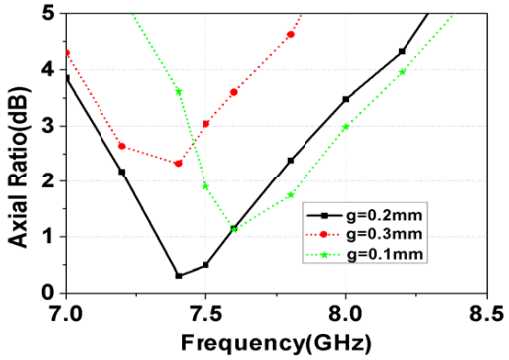

Figure 9. Effect of g on ARBW.

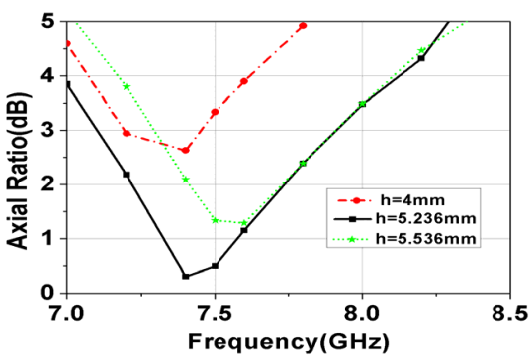

Figure 10. Effect of h on ARBW.

bandwidth covers the frequency range from 7.1 to 7.9 GHz.

Figure 11 depicts the effect on AR bandwidth performance by varying the values of $dr1$ and $dr9$. Circularly polarized characteristics have been realized by removing the corners ($dr1$ & $dr9$) of both the DRs at 45°. From Fig. 11, it is seen that the AR bandwidth gets enhanced after etching the corner of DRs ($dr1$ and $dr9$).

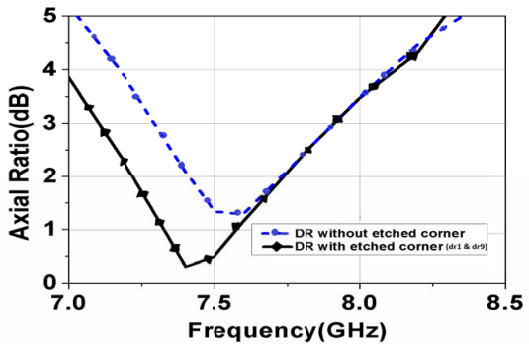

Figure 11. Effect of $dr1$ & $dr9$ on ARBW.

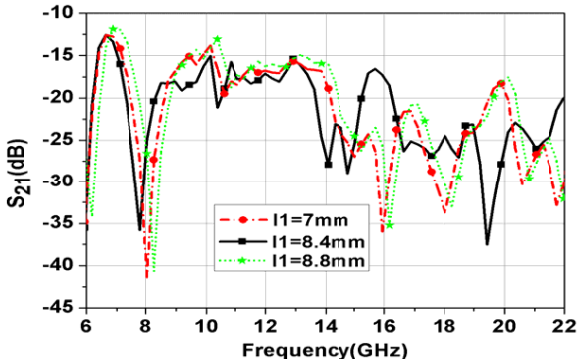

Figure 12. Effect of $l1$ on S_{21} characteristics.

In the previous Fig. 3(b), it is already seen that S_{21} is less than −10 dB in the case of a conventional ground plane. Therefore, to improve the isolation (< −15 dB), a Y-shaped stub along with two L-shaped parasitic strips has been used. The critical point is to design a compact MIMO antenna without disturbing antenna performances. To do that, mutual coupling or isolation between radiating elements is a key factor. So, isolation mechanism plays an important role in MIMO antenna. Fig. 12 demonstrates the effectiveness of the decoupling on S_{21} characteristics by varying the length of L-shaped parasitic strip ($l1$), which has been implemented on the ground plane. A parametric investigation has been carried out in order to evaluate the wideband decoupling mechanism.

As the length of $l1$ changes from 7 mm to 8.4 mm, it is seen that the isolation gets improved, which is better than −15 dB over the entire frequency range of 7.1–22 GHz. As the length of $l1$ changes from 8.4 mm to 8.8 mm, the decoupling bandwidth gets shifted towards the upper-end frequency, which degrades the isolation between the two ports. Thus, the optimum value of $l1$ has been chosen to be 8.4 mm.

Figure 13 demonstrates the effect on S_{21} characteristics by varying the value of the Y-shaped stub (yw). As the value of yw changes from 0.5 mm to 0.3 mm, it is observed that the isolation is less than 10 dB, which is not acceptable. It is noticed that the isolation has been slightly improved (less than 12 dB) as the value of yw further changes from 0.5 mm to 1 mm. Thus, it can be concluded that the optimum value of yw is 0.5 mm so as to achieve better isolation, which is less than −15 dB.

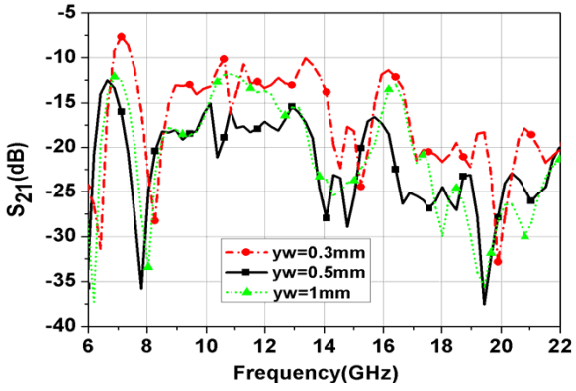

Figure 13. Effect of yw on S_{21} characteristics.

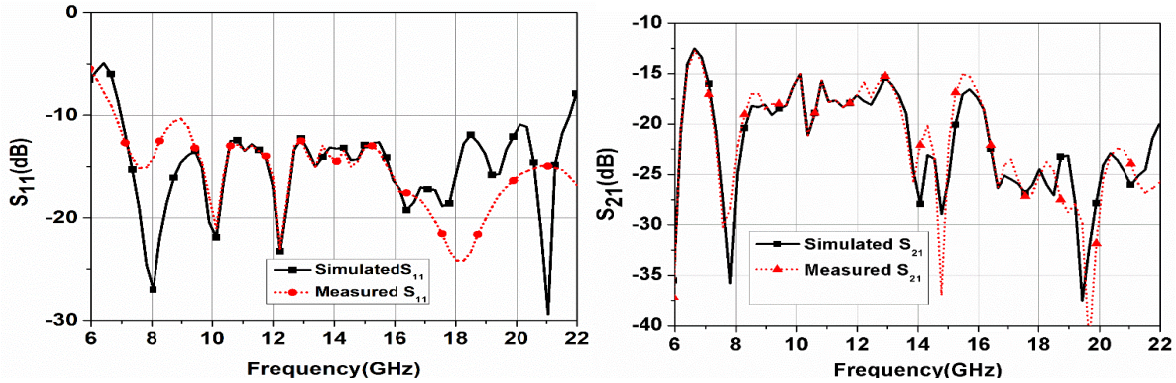

(a) (b)

Figure 14. (a) Measured S_{11} bandwidth characteristics. (b) Measured S_{21} bandwidth characteristics.

Figures 14(a)–(b) show the measured S_{11} and S_{21} characteristics of the designed antenna. A slight discrepancy has been observed between simulated and measured results but with a reasonable agreement between them. The proposed antenna achieves a wide impedance bandwidth of 7.1–22 GHz and low mutual coupling of less than −15 dB within the entire frequency range.

The fabricated prototype of the proposed antenna is shown in Figs. 15(a), (b).

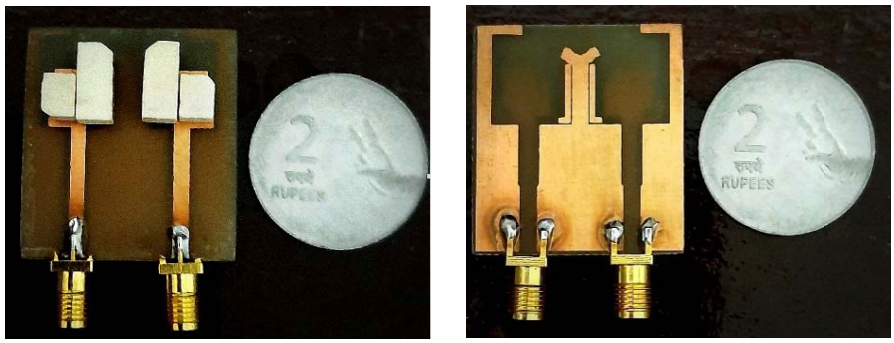

(a) (b)

Figure 15. Fabricated prototype of the proposed antenna. (a) Front view, (b) back view.

Figure 16 presents the simulated and measured AR characteristics which are in good agreement. It is seen that the antenna achieves circular polarization characteristics, which covers the frequency range of 7.1–7.9 GHz.

Envelope correlation coefficient (ECC) is an important parameter to analyze the performance of a MIMO antenna. ECC is a critical diversity performance metric that tells how much field correlation is there in between the different antenna elements of a MIMO system. It depicts how the radiation patterns of each antenna element interact when all ports are active at the same time. The ECC of the proposed MIMO antenna can be calculated by using [30] Equation (4).

$$\mathrm{ECC} = \frac{\left|\iint 4\pi \left[\overrightarrow{F1}\left(\theta,\varphi\right) * \overrightarrow{F2}\left(\theta,\varphi\right)\right] d\Omega\right|^2}{\iint 4\pi \left|\overrightarrow{F1}(\theta,\varphi)\right|^2 d\Omega \iint 4\pi \left|\overrightarrow{F2}(\theta,\varphi)\right|^2 d\Omega} \tag{4}$$

Here, $Fi(\theta,\phi)$ is the three-dimensional field radiation pattern of the designed antenna when the ith port is excited, and Ω is the solid angle. If the radiations patterns of the MIMO antenna are identical,

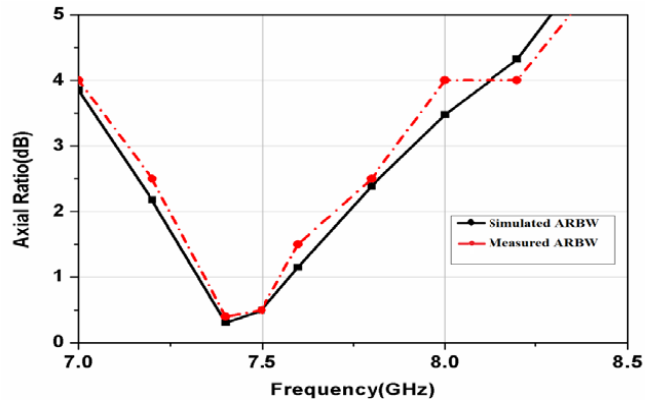

Figure 16. Measured axial ratio characteristics.

then the correlation coefficient would be 1. If they are completely independent, then it will become 0. It is seen that the ECC value lower than 0.03 shows good diversity of the proposed antenna. For an uncorrelated diversity antenna, the ideal value of ECC should be zero [35], but the practical, acceptable value is less than 0.03 for 4G wireless systems, which is achieved and shown in Fig. 17.

Diversity gain is a measure of the effectiveness of diversity on the communication system. This term represents the dissimilarity among the time-averaged Signal to Noise Ratio of the combined signals within the diversity antenna system and that of a single antenna system in one diversity channel. The value of diversity gain [31] for the proposed antenna using ECC can be calculated by using Equation (5).

$$\mathrm{DG} = 10\sqrt{10 - \mathrm{ECC}^2} \tag{5}$$

Figure 17 presents the variation of ECC and diversity gain performances with respect to frequency. From the figure, it is seen that the ECC is below 0.03, while the diversity gain is almost 10 dB throughout the entire frequency range of 7.1 GHz to 22 GHz. Hence, it can be concluded that the MIMO antenna parameter ensures satisfactory spatial multiplexing performance, which in turn ensures enhanced data rate too.

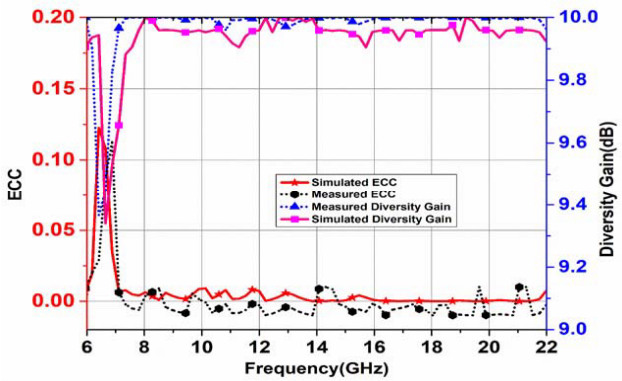

Figure 17. ECC and diversity gain of the proposed MIMO antenna.

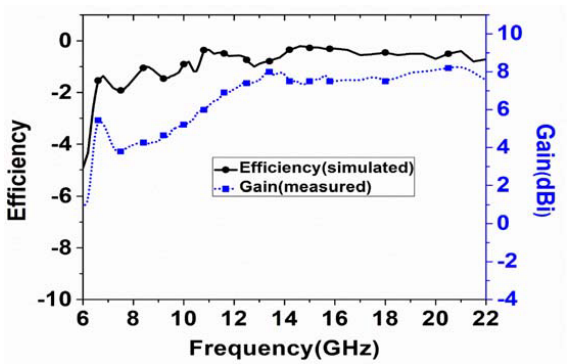

Figure 18. Gain & efficiency of the proposed antenna.

Figure 18 presents measured gain and simulated efficiency of the proposed antenna. The efficiency of the antenna is almost 70% at the lower end frequency and close to 80% at the upper end. The measured gain varies from 4 dBi to 7 dBi over the entire frequency of 7.1 GHz to 22 GHz.

Figure 19 presents the normalized radiation pattern characteristics of the proposed MIMO antenna at 7.2 GHz and 7.8 GHz, including LHCP and RHCP components. Since the two antenna elements are identical, the radiation pattern of Ant.1 is measured, while port 2 is terminated with a 50 Ω load. The

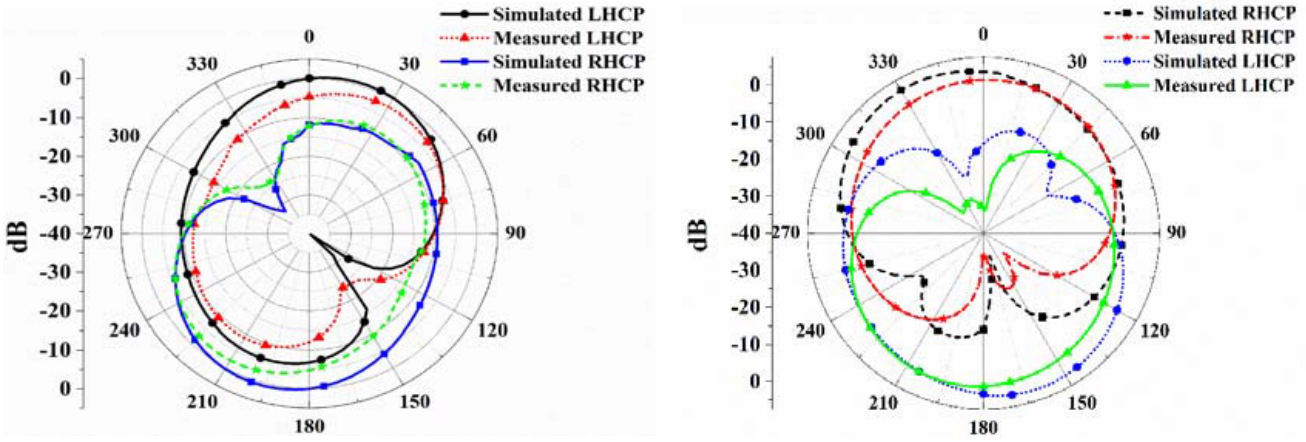

(a) (b)

Figure 19. Radiation pattern characteristics at (a) 7.2 GHz, (b) 7.8 GHz.

radiation patterns are not omnidirectional, as the proposed antenna is not symmetrical and is impacted by stubs and slots in the monopole. Due to fabrication tolerances and antenna chamber mounting arrangements, there may be some minor variations, though the measured and simulated results are in reasonable agreement.

Table 2 represents the comparison of the proposed circularly polarised Dielectric Resonator MIMO antenna with other related MIMO antennas. It is seen that a circularly polarized MIMO antenna has been introduced in [1], whose impedance bandwidth is much lower than the proposed antenna. Also the AR bandwidth and impedance bandwidth characteristics of the antenna presented in [3] are much lower than the proposed antenna. In [5, 8, 9, 33, 34], the sizes of the antennas are much larger, and also the impedance bandwidth is much lower than the proposed antenna. It is seen that most of the works based on MIMO do not produce CP characteristics, but the proposed antenna does. As a whole, the proposed antenna is compact compared to the other referred antennas and also achieves impedance bandwidth which covers the frequency range of 7.1–22 GHz (106%) and AR bandwidth, which covers the lower frequency of 7.1–7.9 GHz (10.6%). This antenna can be effectively used as a dual polarized antenna based on the operating frequency.

Table 2. Comparison of the proposed antenna with other related antennas.

References	Size (mm^3)	−10 dB impedance bandwidth (%)	Axial Ratio Bandwidth (%)	Isolation (dB)
[1]	13.7 × 13.2 × 0.635	5.2–6.3 GHz (18.3%)	5.2–6.3 GHz (18.3%)	−22 dB
[3]	27.69 × 97 × 1.524	5.49–6.024 GHz (12.3%)	5.74–5.83 GHz (0.8%)	−33 dB
[8]	55 × 59 × 8.1	3–7 GHz (80%)	not available	−18 dB
[5]	34 × 32 × 1.53	0.8–1 GHz (22%)	not available	not available
[9]	80 × 80 × 1.6	2.56–2.64 GHz (3%)	not available	not available
[33]	48 × 70 × 1.6	1.86–2.60 GHz, 3.3–3.64 GHz and 4.42–6.75 GHz	not available	−18 dB
[34]	55 × 59 × 1.6	3–7 GHz (80%)	not available	−18 dB
Proposed MIMO antenna	30 × 33 × 0.762	7.1–22 GHz (106%)	7.1–7.9 GHz (10.6%)	−18 dB

5. CONCLUSION

This article describes the design steps of a dual-port Dielectric Resonator-based circularly polarized MIMO antenna for wideband applications such as Radar applications and Ku band. The proposed antenna covers the bandwidth of 7.1–22 GHz (106%) with good isolation below −15 dB within the entire frequency band. The antenna also achieves circular polarization characteristics which covers the frequency range of 7.1–7.9 GHz (10.6%). The ECC and diversity gain performances of the proposed MIMO antenna is within the acceptable threshold limit, which is required for enhancing the data rate through spatial multiplexing in wireless communication channels. Moreover, after observing all the results, it can be concluded that the dual-port MIMO antenna can be a good candidate for different wideband applications.

REFERENCES

1. Ullah, U., I. B. Mabrouk, and S. Koziel, "Enhanced-performance circularly polarized MIMO antenna with polarization/pattern diversity," *IEEE Access*, Vol. 8, 11887–11895, 2020.
2. Thai, P. K., H. Huang, and T. T. Le, "Circular polarized MIMO antenna utilizing parasitic elements for simultaneous improvements in isolation, bandwidth and gain," *International Journal of Electronics and Communications*, Vol. 135, 153727, 2021.
3. Malviya, L., R. K. Panigrahi, and M. Kartikeyan, "Circularly polarized 2×2 MIMO antenna for WLAN applications," *Progress In Electromagnetics Research C*, Vol. 66, 97–107, 2016.
4. Dwivedi, A. K., A. Sharma, A. K. Pandey, et al., "Two port circularly polarized MIMO antenna design and investigation for 5G communication systems," *Wireless Personal Communication*, Vol. 66, 2021.
5. Alexa, F., B. Bardeanu, and D. Vatau, "MIMO antenna system for LTE," *International Conference on Telecommunications and Signal Processing*, 294–298, 2020.
6. Larsson, E. G., O. Edfors, F. Tufvesson, and T. L. Marzetta, "Massive MIMO for next generation wireless systems," *IEEE Communications Magazine*, Vol. 52, No. 2, 186–195, 2014.
7. Lee, S., S. Kim, K. Lee, and Y. Kim, "MIMO antenna using a ground plane protruding for WCDMA application," *Asia-Pacific Microwave Conference*, 574–577, 2011.
8. Kumari, T., G. Das, A. Sharma, and R. K. Gangwar, "Design approach for dual element hybrid MIMO antenna arrangement for wideband applications," *Int. J. RF Microwave Computer Aided Eng.*, Vol. 4, 1–10, 2018.
9. Nasir, J., M. H. Jamaluddin, M. Khaily, M. R. Kamarudin, and I. Ullah, "Design of a MIMO dielectric resonator antenna for 4G applications," *Wireless Personal Communication*, Vol. 3, 525–536, 2016.
10. McAllister, M. W., S. A. Long, and G. L. Conway, "Rectangular dielectric resonator antenna," *Proceedings of the International Symposium Digest — Antennas and Propagation*, Vol. 21, No. 3, 696–699, 1983.
11. Mongia, R. K., A. Ittibipoon, and M. Cuhaci, "Low profile dielectric resonator antennas using a very high permittivity material," *Electronics Letters*, Vol. 30, No. 17, 1362–1363, 1994.
12. Mongia, R. K. and P. Bhartia, "Dielectric resonator antennas — A review and general design relations for resonant frequency and bandwidth," *Int. J. RF Microwave Computer Aided Eng.*, Vol. 4, 230–247, 1994.
13. Mongia, R. K. and A. Ittpibon, "Theoritical and experimental investigations on rectangular dielectric resonator antenna," *IEEE Transactions on Antennas and Propagation*, Vol. 45, No. 9, 1348–1356, 1997.
14. Kishk, A. and K. F. Lee, "Comparative study on different feeding techniques for dual polarized dielectric resonator antenna," *Antennas and Propagation Society International Symposium*, 2006.
15. Denidni, T. A. and Z. Weng, "Hybrid ultra wideband dielectric resonator antenna and band notched designs," *IET Microwave Antennas Propagation*, Vol. 4, 450–458, 2011.

16. Yan, J. B. and J. T. Berhard, "Design of a MIMO dielectric resonator antenna for LTE femtocell base stations," *IEEE Transactions on Antennas and Propagation*, Vol. 4, No. 2, 438–444, 2012.
17. Petosa, A., *Dielectric Resonator Antenna Handbook*, Artech House, Norwood, MA, 2007.
18. Karmakar, A., P. Chakraborty, U. Banerjee, and A. Saha, "Combined triple band circularly polarised and compact UWB monopole antenna," *IET Microwaves, Antennas & Propagation*, Vol. 13, No. 9, 1306–1311, 2019.
19. Banerjee, U., A. Karmakar, and A. Saha, "A review on circularly polarized antennas, trends and advances," *International Journal of Microwave and Wireless Technologies*, Vol. 12, No. 9, 922–943, 2020.
20. Kumar, R. and R. K. Chaudhary, "A wideband circularly polarized cubic dielectric resonator antenna excited with modified microstrip feed," *IEEE Antennas and Wireless Propagation Letters*, Vol. 15, 1285–1288, 2016.
21. Huang, C. Y., J. Y. Wu, and K. L. Wong, "Cross-slotted coupled microstrip antenna and dielectric resonator antenna for circular polarization," *IEEE Transactions on Antennas and Propagation*, Vol. 47, No. 4, 605–609, 1999.
22. Khoo, K. W., Y. X. Guo, and L. C. Ong, "Wideband circularly polarized dielectric resonator antenna," *IEEE Transactions on Antennas and Propagation*, Vol. 55, No. 7, 1929–1932, 2007.
23. Chair, R., S. L. S. Yang, A. A. Kishk, K. F. Lee, and K. M. Luk, "Aperture fed wideband circularly polarized rectangular stair shaped dielectric resonator antenna," *IEEE Transactions on Antennas and Propagation*, Vol. 54, No. 2, 1350–1352, 2006.
24. Lu, L., Y. C. Jiao, W. Liang, and H. Zhang, "A novel low-profile dual circularly polarized dielectric resonator antenna," *IEEE Transactions on Antennas and Propagation*, Vol. 64, No. 5, 4078–4083, 2016.
25. Fakhte, S., H. Oraizi, and R. Karimian, "A novel low-cost circularly polarized rotated stacked dielectric resonator antenna," *IEEE Antennas and Wireless Propagation Letters*, Vol. 13, 722–725, 2014.
26. Altaf, A., Y. Yang, K. Y. Lee, and K. C. Hwang, "Circularly polarized Spidron fractal dielectric resonator antenna," *IEEE Antennas and Wireless Propagation Letters*, Vol. 14, 1806–1809, 2015.
27. Kumar, R., R. Chowdhury, and R. K. Chaudhary, "A new dual mode wideband circularly polarized rectangular dielectric resonator antenna coupled with stubs and asymmetric ground plane for WiMAX applications," *Int. J. RF Microwave Computer Aided Eng.*, Vol. 27, No. 7, 1–7, 2017.
28. Elfergani, I., J. Rodriguez, A. Iqbal, M. Sajedin, C. Zebiri, and R. A. Abd Alhameed, "Compact millimeter-wave MIMO antenna for 5G applications," *14th European Conference on Antennas and Propagation (EuCAP)*, 1–5, 2020.
29. Kareemulla, S. and V. Kumar, "A novel compact MIMO antenna for ultra wideband applications," *IEEE International Conference on Signal Processing, Informatics, Communication and Energy Systems (SPICES)*, 1–5, 2015.
30. Sharawi, M. S., "Printed multi-band MIMO antenna systems and their performance metrics," *IEEE Antennas Propag. Mag.*, Vol. 55, No. 5, 218–23, 2013.
31. Blanch, S., J. Romeu, and I. Corbella, "Exact representation of antenna system diversity performance from input parameter description," *Electronics Lett.*, Vol. 39, No. 9, 705–707, 2003.
32. Gao, Y., Z. Feng, and L. Zhang, "Compact CPW-fed dielectric resonator antenna with dual polarization," *IEEE Antennas and Wireless Propagation Letters*, Vol. 10, 544–547, 2011.
33. Das, G., A. Sharma, and R. K. Gangwar, "Triple band hybrid antenna with integral isolation mechanism for MIMO applications," *Microwave and Optical Technology Letters*, Vol. 60, No. 6, 1482–1491, 2017.
34. Kumari, T., G. Das, and R. K. Gangwar, "Design approach for dual element hybrid MIMO antenna arrangement for wideband applications," *RF and Microwave Computer Aided Engineering*, Vol. 29, No. 1, 2018.
35. Nandi, S. and A. Mohan, "A compact dual-band MIMO slot antenna for WLAN applications," *IEEE Antennas and Wireless Propagation Letters*, Vol. 16, 2457–2460, 2017.